CHEMISTRY
A EUROPEAN JOURNAL

DOI: 10.1002/chem.200801895

EPR Spectroscopy of a Family of $Cr^{III}_7M^{II}$ (M = Cd, Zn, Mn, Ni) "Wheels": Studies of Isostructural Compounds with Different Spin Ground States

Stergios Piligkos,*[a, b, e] Høgni Weihe,[a] Eckhard Bill,[b] Frank Neese,[b, c] Hassane El Mkami,[d] Graham M. Smith,[d] David Collison,[e] Gopalan Rajaraman,[e, f] Grigore A. Timco,[e] Richard E. P. Winpenny,[e] and Eric J. L. McInnes[e]

Abstract: We present highly resolved multifrequency (X-, K-, Q- and W-band) continous wave EPR spectra of the heterooctametalic "wheels", $[(CH_3)_2NH_2][Cr^{III}_7M^{II}F_8((CH_3)_3CCOO)_{16}]$, hereafter Cr_7M, where M = Cd, Zn, Mn, and Ni. These experimental spectra provide rare examples of high nuclearity polymetallic systems where detailed information on the spin-Hamiltonian parameters of the ground and excited spin states is observed. We interpret the EPR spectra by use of restricted size effective subspaces obtained by the rigorous solution of spin-Hamiltonians of dimension up to 10^5 by use of the Davidson algorithm. We show that transferability of spin-Hamiltonian parameters across complexes of the Cr_7M family is possible and that the spin-Hamiltonian parameters of Cr_7M do not have sharply defined values, but are rather distributed around a mean value.

Keywords: davidson algorithm · effective subspaces · EPR spectroscopy · heterometallic wheels · *S*-mixing

[a] Dr. S. Piligkos, Dr. H. Weihe
Department of Chemistry, University of Copenhagen
Universitetsparken 5, 2100 Copenhagen (Denmark)
Fax: (+45) 3532-0133
E-mail: piligkos@kiku.dk

[b] Dr. S. Piligkos, Dr. E. Bill, Prof. Dr. F. Neese
Max-Plank-Institut für Bioanorganische Chemie
Stiftstrasse 34–36, 45470 Mülheim (Germany)

[c] Prof. Dr. F. Neese
Present address:
Institut für Physikalische und Theoretische Chemie
University of Bonn, Wegelerstrasse 12
53115 Bonn (Germany)

[d] Dr. H. El Mkami, Dr. G. M. Smith
School of Physics and Astronomy, University of St Andrews
North Haugh, KY16 SS, St. Andrews (UK)

[e] Dr. S. Piligkos, Prof. D. Collison, Dr. G. Rajaraman, Dr. G. A. Timco, Prof. R. E. P. Winpenny, Prof. E. J. L. McInnes
School of Chemistry, The University of Manchester
Oxford Road, M13 9PL, Manchester (UK)

[f] Dr. G. Rajaraman
Present address:
Laboratory of Molecular Magnetism
Dipartimento di Chimica e UdR INSTM, di Firenze
Polo Scientifico, Via della, Lastruccia 3
50019 Sesto Fiorentino, Fi (Italy)

Supporting information for this article is available on the WWW under http://dx.doi.org/10.1002/chem.200801895: Calculated contributions, from the two lowest eigenstates, to the EPR spectrum of **1** at 180 GHz, Q-dependences and INS spectra of **1**, **2**, and **3** computed with the spin-Hamiltonian parameters of Table 1, determined in this work, and colour version of Figures 3–6, 8–10, 13, 14.

Introduction

Understanding the magnetic properties of polymetallic exchange coupled systems requires a detailed insight into the magnetic properties of their elementary building blocks (single-ion terms) and the interactions between them (exchange terms). This information is in principle accessible when well-resolved spectroscopic data originating from numerous spin states of the system studied are experimentally observed since single-ion and exchange terms project differently on the ground and various excited spin states. Electron paramagnetic resonance (EPR) spectroscopy can offer the required spectral resolution to allow for a detailed analysis of the magnetic properties of exchange coupled systems in terms of single-ion and exchange contributions. However, well-resolved EPR data containing detailed information on excited spin states of exchange coupled systems are rare due to line broadening because of factors such as fast spin relaxation. Highly resolved EPR spectra of oxo- and hydroxo-bridged Cr^{III} and Fe^{III} binuclear complexes have been reported.[1,2] In these studies the spin-Hamiltonian parameters of the ground and excited spin states were determined and their origin discussed in terms of single-ion and exchange contributions by use of spin projection[3] or full matrix diagonalisation approaches. The diamagnetic substitution approach, that is, investigation of doped diamagnetic analogues, has been used in some of these studies[1b,c,2b] for the

direct determination of single-ion terms. Although this approach is very difficult to apply to polymetallic systems because of obvious difficulties related to the synthesis of monosubstituted complexes, such an approach has been reported in the study of an hexanuclear iron(III) complex where the EPR resonances from the Fe^{III} monosubstituted hexanuclear gallium(III) analogue allowed for the quantification of single-ion contributions to the spin-Hamiltonian parameters of the hexanuclear Fe^{III} complex.[4] EPR transitions within excited spin states have been reported for another hexanuclear cyclic Fe^{III} complex[5] and for a nonanuclear Mn^{II} complex.[6] In the case of the cyclic Fe^{III}_6 complex the spectra were interpreted by considering single-ion and dipolar and anisotropic exchange terms to the full spin-Hamiltonian of the system that was diagonalised by use of irreducible tensor operator (ITO) techniques coupled to a group theoretical treatment.[5] In the case of the Mn^{II}_9 complex the EPR spectra were modelled by use of an effective lower-dimension spin-Hamiltonian matrix constructed on the basis of a reduced spin model representing the full system.[6]

We present here highly resolved multifrequency (X-, K-, Q- and W-band) continuous wave EPR spectra obtained on single crystals and polycrystalline samples of a family of the heterometallic "wheels", $[(CH_3)_2NH_2][Cr^{III}_7M^{II}F_8((CH_3)_3CCOO)_{16}]$,[7] hereafter Cr_7M, where M = Cd (**1**), Zn (**1′**), Mn (**2**), and Ni (**3**). The molecular structure of the Cr_7M "wheels" is shown in the left panel of Figure 1. The experimental spectra provide rare examples of high nuclearity polymetallic systems where detailed information on the spin-Hamiltonian parameters of the ground and several excited spin states is experimentally observed. Furthermore, the fact that the Cr_7M complexes are isostructural and of nearly identical chemical nature, allows an investigation to be carried out of the transferability of spin-Hamiltonian parameters between complexes.

The theoretical interpretation of the EPR spectra presented here cannot be performed by a full-matrix diagonalisation approach because of the large dimension of the spin-Hamiltonian matrices and the requirement, for EPR, to repeatedly diagonalise over magnetic field and orientation degrees of freedom. Even on large computers, traditional full-matrix diagonalisation techniques are limited to matrix dimensions of the order of 10^4. The problem of diagonalisation of very large spin-Hamiltonian matrices has been previously approached by use of ITO techniques, group theoretical treatments and the sparse matrix Lanczos diagonalisation algorithm.[5,8–10] In addition, lower-dimension effective spin-Hamiltonian operators based on reduced spin model representations of the full systems have been employed to deal with the same problem.[6,11]

We have recently developed a method for the interpretation of static thermodynamic and spectroscopic properties of large polymetallic systems based on the use of the Davidson numerical diagonalisation algorithm.[12] In a recent communication, we briefly outlined our approach for the interpretation of low frequency (X-, K-, and Q-band) EPR spectra obtained on **1**.[13] In this work, we discuss in detail the developed approach for the interpretation of low- and high-frequency EPR spectra for the series of Cr_7M complexes, characterized by spin-Hamiltonian matrices of dimension up to 10^5, as well as the transferability of spin-Hamiltonian parameters between complexes.

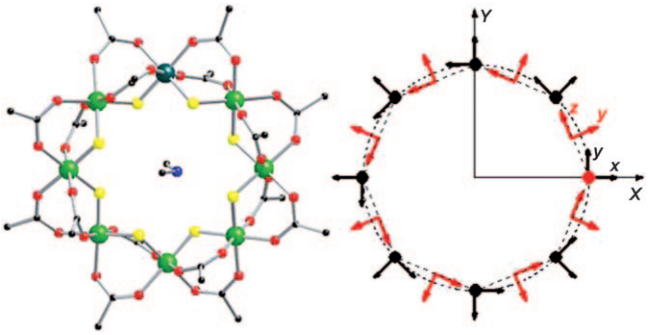

Figure 1. nLeft panel: Molecular structure of the Cr_7M complexes. Colours: Cr^{III} (green), M^{II} (dark olive-green), F (yellow), O (red), C (black), N (blue). The heterometal M^{II} site is disordered and its different color is for aesthetic reasons. CH_3 groups from $(CH_3)_3CCOO$ and H atoms from $(CH_3)_2NH_2$ were omitted for clarity. Right panel: Geometric representation of the orientation of the anisotropy tensors included in spin-Hamiltonian (2). The metal centres are in the (xy) plane of the molecular reference frame (xyz), the z axis being normal to the plane of the ring. The seven Cr^{III} centres are depicted as solid black discs, their indices running from 1 to 7. The M^{II} site is depicted as a solid red disc of index 8. The local reference systems (xyz) of the single-ion anisotropy tensors are depicted in black. Their z component is normal to the plane of the ring and they transform into each other by successive rotations of 45° about the molecular z axis. The dimer anisotropic exchange local reference systems (xyz) are depicted in red and they transform to each other in the same way. Their z components are directed along the intermetallic distance direction.

The Cr_7M molecules are analogues of the octanuclear Cr^{III} ring, $[Cr^{III}_8F_8((CH_3)_3CCOO)_{16}]$,[14] hereafter, Cr_8. The homometallic Cr_8 has a diamagnetic $S=0$ ground spin state as a consequence of antiferromagnetic exchange interactions between neighbouring Cr^{III} centres.[8,15] In Cr_7M, the presence of the M^{II} centre substituting for one Cr^{III} centre of the parent Cr_8 does not alter the antiferromagnetic nature of the magnetic exchange interactions in the molecule. Consequently, given that the Cr^{III} single-ion electronic spin is $S_{Cr^{III}}=3/2$, the Cr_7M "wheels" have paramagnetic ground spin states of total spin $S=3/2$ for **1** and **1′** ($S_{Cd^{II}} = S_{Zn^{II}}=0$), $S=1$ for **2** ($S_{Mn^{II}}=5/2$), and $S=1/2$ for **3** ($S_{Ni^{II}}=1$), as has previously been shown by magnetic susceptibility,[7] and detailed inelastic neutron scattering[9] (INS) measurements. Thus, this series of isostructural complexes offers the possibility to study the magnetic behaviour of spin states of different total spin, which are closely related with respect to their origin, within a constant structural motif where the only variation resides in the identity of the M^{II} centre.

The presence of the M^{II} centre lowers the symmetry of the Cr_7M complexes, compared to the parent Cr_8, and in combination with inter-spin-state mixing (S-mixing) effects is responsible for these complexes showing quantum oscillations of the total spin of specific spin eigenstates at level anti-crossings[16,17] at certain strengths and orientations of an

externally applied magnetic field. This has been observed on single crystals of Cr_7M complexes by torque magnetometry[16] and INS.[17] The Cr_7M complexes have also been proposed as possible physical supports for the implementation of quantum computing algorithms.[18] Pulsed electron paramagnetic resonance (EPR) measurements[19] performed on per-deuterated analogues of **3** have shown that its $S=1/2$ ground spin state displays a phase coherence time T_2 of 3.8 μs at 1.8 K, "exceeding by two orders of magnitude the timescale of coherent manipulations of the electron spin with existing apparatus".[19]

Results and Discussion

Models used for the interpretation of the experimental EPR data of Cr_7M: The traditional approach for the interpretation of the experimental EPR data of Cr_7M would be to consider the spectra as a sum of contributions from independent spin states of total spin *S*. The relevant spin states for such a model can be easily determined for Cr_7M by use of previously determined isotropic exchange parameters[7,9] and ITO algebra techniques. However, such an approach to the EPR spectra of Cr_7M is intrinsically problematic because the unusually good resolution means that we would have to independently model up to the fourth or fifth excited state, sometimes based on the observation of only a few resonances. This generates a lot of independent parameters. Moreover, analysing these parameters via projection coefficients in order to determine single-ion and exchange terms involves the assumption that *S*-mixing[20] effects are negligible. Such *S*-mixing effects strongly depend on the presence of single-ion and exchange anisotropy terms in the spin-Hamiltonian of the system and, to second order in perturbation theory, are inversely proportional to the energy gap between admixed spin states.

In recent work Hill and Hendrickson outlined the limitations of the giant spin approximation (GSA), that consists of considering the ground spin state of an exchange coupled system as thermally isolated and presenting no interactions with excited spin states, in interpreting the EPR data of a $\{Ni_4\}$ cubane.[21] A particular focus of their analysis concerned the necessity of accounting for exchange-controlled *S*-mixing effects by introducing additional, higher order terms to the usual form of the GSA spin-Hamiltonian. *S*-mixing effects were also found to be important in the interpretation of EPR data of an Fe^{III} binuclear complex where it was shown that the projection coefficients of the single-ion and exchange anisotropy, determined within the strong exchange limit model, are not sufficient to reproduce the experimental spectra.[2b] Very recently, Barra et al.[11] demonstrated that in an axially symmetric dodecanuclear $Mn^{III}_8Mn^{IV}_4$ complex, *S*-mixing effects induce the presence of diagonal and off-diagonal anisotropy terms up to sixth order to the GSA spin-Hamiltonian. *S*-mixing effects were also found to be important for the interpretation of the EPR resonances of a cyclic Fe^{III}_6 complex.[5] Finally, *S*-mixing effects were shown to be important for the description of the magnetic properties of the $S=12$ ground spin state of an hexanuclear Mn^{III} complex displaying the highest barrier yet observed to the reversal of the magnetization upon removal of an external magnetic field.[22] Consequently, to model the EPR spectra of Cr_7M as a superposition of contributions originating from independent spin states of total spin *S*, we would have to construct a model that incorporates not only a set of spin-Hamiltonian parameters for each experimentally observed spin state but also parameters corresponding to off-diagonal matrix elements between spin states, in order to take into account any *S*-mixing effects. One can easily see that such a model would require a very large number of parameters, making the results obtained from the analysis of the EPR spectra of Cr_7M of limited value.

To go beyond these limitations and compute exactly spin expectation values of, or transition moments between, thermally populated eigenstates it is necessary to diagonalise numerically the full spin-Hamiltonian matrix of the system of dimension $N=\prod(2S_i+1)$, with S_i the spin quantum number of the *i*th paramagnetic centre of the system. Numerical diagonalisation of large matrices by full-matrix algorithms is currently prohibited by unrealistic computation time and memory storage requirements. However, only a few thermally populated eigenstates have to be taken into account for the description of the low-temperature magnetic and spectroscopic properties of polymetallic systems. To circumvent the above technical limitations we adapted to the spin-Hamiltonian formalism an iterative approach that exploits the sparse nature of the Hamiltonian matrix, known as the Davidson algorithm.[12] The Davidson algorithm is an iterative subspace diagonalisation approach that allows the exact computation of a number of low-lying eigenstates of the full spin-Hamiltonian of the system starting from a set of, in principle arbitrarily chosen, guess vectors within realistic computation times and memory storage requirements. This approach, as with any other method which provides exact eigenstates numerically,[5,6,10,21] allows for any spin-Hamiltonian term to be included in the spin-Hamiltonian of the system and for all terms to be treated simultaneously and not in a sequential perturbation way. Thus, the methodology used allows for the simultaneous inclusion of single-ion and exchange anisotropy terms, as well as of any other relevant terms, in the spin-Hamiltonian without requiring that the total spin *S* is a good quantum number. The converged low-lying eigenvectors, each of dimension *N*, may directly be used to compute quantities such as spin expectation values or transition moments. Alternatively, they may be used in a unitary transformation of the full Hamiltonian to generate an effective operator accurate in the subspace defined by the converged eigenvectors.

Simple models containing a minimum number of independent parameters are necessary for the meaningful interpretation of the magnetic properties of large polymetallic systems since over-parameterized models can be easily constructed given the multitude of options of possible interac-

tion and single-ion terms. Based on the geometric characteristics of the Cr_7M "wheels" we assume the molecular quantization axis to be normal to the plane of the ring and a first neighbour topology of magnetic exchange interactions. In the case that the protonated secondary amine cation is dimethylammonium, the Cr_7M complexes crystallize in the *P*4 space group with the molecules located on fourfold symmetry sites.[7] There is only one molecular magnetic site per unit cell. Within the molecules, the metal ions are located on the vertices of an octagon with site occupancy $^7/_8$ and $^1/_8$ for Cr^{III} and M^{II}, respectively. The first neighbour intermetallic distances are equivalent and of the order of 3.4 Å. At this distance, within the point dipole approximation, dipolar through-space spin–spin interactions have a negative principal component along the intermetallic vector of magnitude of the order of $-0.1\ cm^{-1}$. The dipolar through-space spin-spin interaction matrix between the *i*th and *j*th single ion-sites can be computed from:[3]

$$\mathbf{D}_{ij}^{\mathrm{dip}} = \frac{\mu_0 \mu_B^2}{4\pi\, r^3}[\boldsymbol{g}_{\mathrm{i}} \cdot \boldsymbol{g}_{\mathrm{j}} - 3(\boldsymbol{g}_i \cdot \mathbf{u})(\mathbf{u} \cdot \boldsymbol{g}_j)] \quad (1)$$

where μ_0 is the magnetic constant or permeability of free space, μ_B is the electron Bohr magneton, *r* is the intermetallic distance, $\mathbf{g}_i$ is the *g* matrix of the *i*th single ion, and **u** is a unit-length vector along the intermetallic direction. Given that the anisotropic exchange contributions are of the same order of magnitude as expected for the single-ion anisotropy terms, they cannot be ignored. Consequently, we include in our spin-Hamiltonian model both single-ion anisotropy and anisotropic exchange terms, the latter representing the sum of through-space dipolar and through-bond anisotropic exchange terms. The single-ion anisotropy tensors, $\mathbf{D}_i$, are assumed to have their largest principal component along the molecular *z* axis, normal to the plane of the "wheel", and one of the two axial components along the radius of the "wheel". This assumption is arbitrary, not imposed by symmetry. However an assumption has to be made at this point given that experimental determination of the exact orientation of the single-ion anisotropy tensors in Cr_7M has not been possible to date. Including the orientation of the single-ion anisotropy tensors as free parameters would obviously result in an over-parameterised model that would render any results of limited value. The assumption made here is not unrealistic since estimation of the Cr^{III} $\mathbf{D}_i$ tensor orientation in the parent Cr_8, by use of the angular overlap model, resulted in a misalignment of the main component (D_{zz}) of about 19° with respect to the molecular *z* axis.[15] The anisotropic exchange tensors, $\mathbf{D}_{ij}$, are assumed to have their largest principal component along the intermetallic vector, in accordance with the orientation of the dipolar spin–spin tensor contributions to the exchange anisotropy, and one of the two axial components along the molecular *z* axis. To further reduce the number of parameters included in our model, we neglect single-ion and exchange rhombic anisotropy terms, antisymmetric exchange terms, and consider isotropic *g* values for all metal centres unless explicitly specified. Neglecting rhombic exchange anisotropy terms and antisymmetric exchange terms appears a well justified choice since there is no experimental evidence for their presence and since their effect would not be clearly discernable from the effect of the terms already included in the model. Neglecting the single-ion rhombic anisotropy terms requires more justification which we will give in later sections.

The above described model is expressed by spin-Hamiltonian (2), where the single-ion terms summations run over all single ions of the system, the exchange terms summations run over first neighbour interactions, **B** is the external applied magnetic field, $\mathbf{g}_i$ is the *g* matrix of the *i*th single-ion site, $\hat{\mathbf{S}}$ is a spin operator, J_{ij} is the isotropic exchange parameter between the *i*th and *j*th single-ion sites, $\mathbf{R}_i$, $\mathbf{R}_{ii}$ and $\mathbf{R}_{ij}$ are the relevant Euler rotation matrices transforming single-ion or dimer local reference systems, respectively, to the molecular reference frame (*xyz*), * denotes complex conjugation, $\mathbf{R}^{-1}$ is the inverse of **R**. In Equation (2) positive and negative J_{ij} correspond to ferromagnetic and antiferromagnetic interactions, respectively. The $\mathbf{D}_i$ and $\mathbf{D}_{ij}$ tensors containing the uniaxial single-ion anisotropy, D_i, and anisotropic exchange, D_{ij}, parameters, respectively, and the $\mathbf{g}_i$ matrices, assumed collinear to $\mathbf{D}_i$, have a diagonal form in their local reference frames. In addition, the $\mathbf{D}_i$ and $\mathbf{D}_{ij}$ tensors are traceless. The geometric characteristics of spin-Hamiltonian (2) that we use in this study for the interpretation of the EPR spectra of the Cr_7M rings are illustrated in the right panel of Figure 1.

$$\begin{aligned}\hat{H}_{aniso} = & \sum_i \mu_B \mathbf{B}\mathbf{R}^*_{g,i}\mathbf{g}_i\mathbf{R}^{-1}_{g,i}\hat{\mathbf{S}}_i \\ & + \sum_i \hat{\mathbf{S}}_i\mathbf{R}^*_{D,ii}\begin{pmatrix} -D_i/3 & 0 & 0 \\ 0 & -D_i/3 & 0 \\ 0 & 0 & 2D_i/3 \end{pmatrix}\mathbf{R}^{-1}_{D,ii}\hat{\mathbf{S}}_i \\ & + \sum_{i,j>i} -2\hat{\mathbf{S}}_i J_{ij}\hat{\mathbf{S}}_j + \sum_{i,j>i}\hat{\mathbf{S}}_i\mathbf{R}^*_{D,ij}\begin{pmatrix} -D_{ij} & 0 & 0 \\ 0 & -D_{ij} & 0 \\ 0 & 0 & 2D_{ij} \end{pmatrix}\mathbf{R}^{-1}_{D,ij}\hat{\mathbf{S}}_j\end{aligned} \quad (2)$$

Previous magnetic susceptibility studies[7] on **1**, and **1′** were modelled using the isotropic spin-Hamiltonian (3),

$$\hat{\mathrm{H}}_{\mathrm{iso}} = -2\sum_{i,j>i}\hat{\mathrm{S}}_i J_{ij}\hat{\mathrm{S}}_j + \sum_i \mu_B \mathbf{B}\, g_{\mathrm{iso},i}\hat{\mathbf{S}}_{\mathrm{i}} \quad (3)$$

where g_{iso} is the isotropic *g* factor of the *i*th site. In these studies magnetic susceptibility data of **1** and **1′** were interpreted within the ITO formalism,[3,23] showing that the isotropic exchange parameter between first-neighbour Cr^{III} centres, $J_{Cr-Cr} = -6.0\ cm^{-1}$. The isotropic exchange parameter between Cr^{III} and Cd^{II} or Zn^{II} sites was set to zero. Given that the magnetic behaviours of **1** and **1′** are equivalent, for the rest of this study we will refer to both compounds as **1**. Magnetic susceptibility data of **2** and **3** could be modelled by using the same J_{Cr-Cr} as for **1**, and the same value for the

J_{Cr-Mn} and J_{Cr-Ni}, respectively.[7] A less symmetric model was not necessary for the modelling of the magnetic susceptibility data. The J_{Cr-Cr} parameter in **1**, **2** and **3** has more recently been more precisely determined by INS studies[9] to be $-5.77\ cm^{-1}$, with $J_{Cr-Cr}=J_{Cr-Mn}$ or J_{Cr-Ni} in **2** and **3**, respectively.[9]

With $J_{Cr-Cr}=-5.77\ cm^{-1}$ at zero applied magnetic field and within an isotropic model, **1** is characterized by an $S=3/2$ ground spin state and lowest-lying $S=1/2$ and $S=5/2$ excited spin states of energy 6.7 and 15.0 cm^{-1} above the ground state, respectively. The zero-field energy spectrum of the twelve lowest lying spin states of **1**, determined with spin-Hamiltonian (3) and with the above isotropic exchange parameter, is shown in Figure 2. These twelve lowest-lying spin

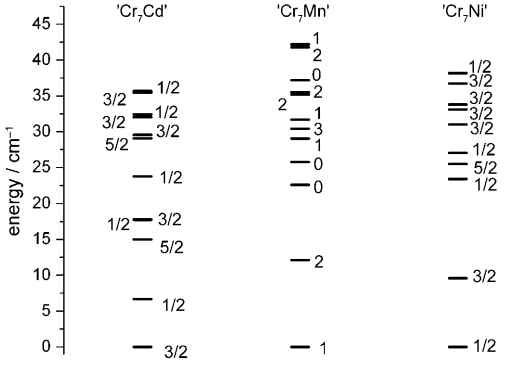

Figure 2. Zero-field energy spectrum of the twelve lowest lying spin states of Cr_7Cd (**1**), of the twelve lowest lying spin states of Cr_7Mn (**2**), and of the ten lowest lying spin states of Cr_7Ni (**3**), determined within the isotropic model of spin-Hamiltonian (3) and with $J_{Cr-Cr}=-5.77\ cm^{-1}$ for **1**, $J_{Cr-Cr}=J_{Cr-Mn}=-5.77\ cm^{-1}$ for **2**, and $J_{Cr-Cr}=J_{Cr-Ni}=-5.77\ cm^{-1}$ for **3**.

states, each of multiplicity $2S+1$, define a subspace spanned by forty-two eigenvectors. The temperature dependence of the summed Boltzmann population within this subspace is shown in Figure 3 as a black trace. From Figure 3 one can see that up to 10 K only eigenstates contained within this subspace have non-negligible Boltzmann population. Consequently, the subspace spanned by the forty-two lowest-lying eigenstates of **1** is sufficient for the reproduction of the resonances observed in the EPR spectra of **1** recorded at temperatures up to 10 K. In the infinite temperature limit all eigenstates of **1** are equally populated. Thus, at high temperatures the summed Boltzmann population within the subspace of the forty-two lowest-lying eigenvectors of **1** tends to the value $42/N$.

In Figure 2 are also shown the zero-field eigenvalues and total spin S of the twelve lowest lying spin states of **2** and of the ten lowest spin states of **3**, assuming $J_{Cr-Mn}=J_{Cr-Cr}=-5.77\ cm^{-1}$ and $J_{Cr-Ni}=J_{Cr-Cr}=-5.77\ cm^{-1}$, respectively. The twelve lowest-lying spin states of **2** define a subspace spanned by forty-two eigenvectors, whereas the ten lowest-lying spin states of **3** define a subspace spanned by thirty-four eigenvectors. The temperature dependence of the summed Boltzmann populations within these subspaces is shown in

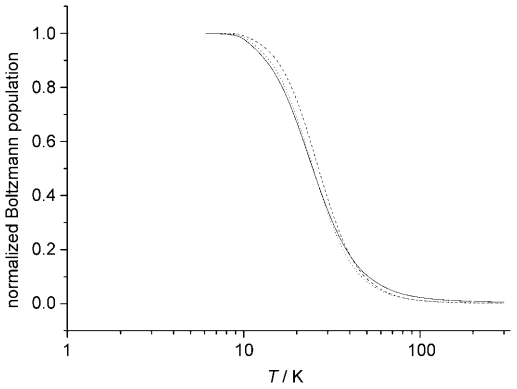

Figure 3. Temperature dependence of the summed Boltzmann population within the subspace defined by the twelve lowest-lying spin states of Cr_7Cd (**1**; ——), the twelve lowest-lying spin states of Cr_7Mn (**2**; -----), and the ten lowest-lying spin states of Cr_7Ni (**3**; •••••), determined within the isotropic model of spin-Hamiltonian (3) and with $J_{Cr-Cr}=-5.77\ cm^{-1}$ for **1**, $J_{Cr-Cr}=J_{Cr-Mn}=-5.77\ cm^{-1}$ for **2**, and $J_{Cr-Cr}=J_{Cr-Ni}=-5.77\ cm^{-1}$ for **3**.

Figure 3. As in the case of **1**, the subspaces defined by the forty-two lowest-lying eigenvectors of **2** and by the thirty-four lowest-lying eigenvectors of **3** are sufficient for the reproduction of the EPR spectra of **2** and **3** up to 10 K.

In our discussion below it is convenient to discuss the consequences of the parameters in spin-Hamiltonian (2) to an effective, strong exchange limit spin-Hamiltonian description. The magnetic properties of the individual total spin states S can be described in terms of the effective spin-Hamiltonian (4).

$$\hat{H}_S=\mu_B\mathbf{B}\mathbf{g}_S\hat{\mathbf{S}}+D_S[\hat{S}_Z^2-S(S+1)/3]+E_s(\hat{S}_X^2-\hat{S}_Y^2)+\sum_{q=0,1,2,3,4}B_4^q\hat{O}_4^q \quad (4)$$

In spin-Hamiltonian (4) $\mathbf{g}_S$ is the g matrix, D_S is the uniaxial anisotropy parameter, E_S is the rhombic anisotropy parameter, and B_4^q is the parameter associated to the $\hat{O}_4^q$ Steven's operator[24] of spin state S. All Steven's operators of even order up to $2S$ can be included in (4). Here Steven's operator terms only up to fourth order are included for simplicity.

The experimental EPR spectra of the Cr_7M complexes, shown in later sections, exhibit bands with markedly different linewidths, Γ. These variable linewidths have been accounted for in the computation of the simulated spectra by use of Equation (5):[25]

$$\Gamma^2=\left(\frac{\Gamma_0}{g'}\right)^2+\sum_p\sigma_p^2\left(\frac{\partial B_r}{\partial p}\right)^2;\ g'=\frac{1}{g_{iso}\mu_B}\frac{\partial\Delta}{\partial B} \quad (5)$$

that expresses the linewidth of a given transition in magnetic field units assuming a Gaussian line-shape function. In Equation (5), Γ_0 is the natural, unbroadened linewidth of the transition, assumed to be represented by a Gaussian line-shape function, p represents a given spin-Hamiltonian

parameter, σ_p is the standard deviation of the Gaussian distribution of the parameter p, B_r is the resonance field of the observed transition, and Δ is the energy difference between the two levels involved in the transition. The first term of Equation (5) expresses the dependence of the linewidth of an observed transition with respect to the derivative of the energy divergence of the states involved in the transition. The second term of Equation (5) expresses the broadening of the line-shape of a given transition because of the existence of a statistical distribution of the value of a given spin-Hamiltonian parameter. The introduction of a Gaussian distribution of a spin-Hamiltonian parameter value expresses the fact that there are slight differences in the environment of the single-ion centres across Cr_7M molecules, the so-called "strain" effects.

Interpretation of the EPR spectra of Cr_7Cd: The Q-band EPR spectra of polycrystalline **1** recorded at 5 and 10 K are shown in Figure 4. The resonances centred at 11.8 and 13.1 kG, marked with *, symmetrically disposed around the "$g=2$" spectral region, present distinctly different temperature variation to the rest of the spectrum. This indicates that excited spin states are being observed.

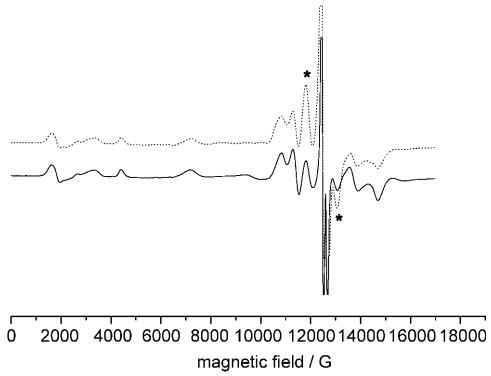

Figure 4. Q-band (34.05 GHz) EPR spectra of polycrystalline Cr_7Cd (**1**) at 5 (——) and 10 K (•••••).

For the simulation of the EPR spectra of **1** we use spin-Hamiltonian (2). The Euler rotation matrices are set by the geometric characteristics, as discussed above. The isotropic exchange parameter J_{Cr-Cr} is fixed to the value determined by INS studies. A simple inspection of the resonance fields of the experimental EPR spectra of **1**, for example the ones shown in Figure 4, allows determination of the isotropic g value of the Cr^{III} sites as $g_{Cr}=1.96$. In this way only two free parameters are contained in spin-Hamiltonian (2), namely the uniaxial single-ion anisotropy, D_{Cr}, and the exchange anisotropy, D_{Cr-Cr}.

As a starting point we set $D_{Cr-Cr}=-0.05\ cm^{-1}$, corresponding to the order of magnitude of the dipolar spin–spin interactions at a distance of 3.4 Å and $D_{Cr}=-0.2\ cm^{-1}$, the order of magnitude of uniaxial single-ion anisotropy derived from INS studies. Application of the spin-Hamiltonian operator (2) to the direct product basis-set functions of **1** results in a Hermitian matrix of dimension $N=16384$ that we diagonalise numerically at zero applied magnetic field by use of the Davidson algorithm to determine the forty-two lowest-lying eigenstates. These forty-two lowest-lying eigenstates are subsequently used as the basis for generation of the matrix representation of spin-Hamiltonian (2), by a unitary transformation, in this effective subspace. The obtained matrix representation of spin-Hamiltonian (2) in the subspace defined by the forty-two lowest-lying eigenstates is then used for the determination of D_{Cr}, and D_{Cr-Cr} by numerical fitting of the observed EPR resonance fields of **1** (polycrystalline and single crystal) at X-, K-, Q-, and W-bands. The best-fit D_{Cr} and D_{Cr-Cr} parameters are then used as a new starting point for the numerical diagonalisation of the full spin-Hamiltonian of the system, of dimension $N=16384$, and the procedure is repeated until no difference is observed between the obtained best-fit D_{Cr} and D_{Cr-Cr} parameters and the D_{Cr} and D_{Cr-Cr} parameters used to generate the matrix representation of spin-Hamiltonian (2) in the effective subspace spanned by its lowest-lying eigenvectors. Thus, the EPR spectra of **1** can be simulated with $D_{Cr}=-0.134\ cm^{-1}$ and $D_{Cr-Cr}=-0.106\ cm^{-1}$ (Table 1; Figures 4–6). The fit of the EPR resonance fields and the computation of EPR spectra were performed by use of home written software.[26]

Table 1. Spin-Hamiltonian parameters used for the computation of the EPR spectra of Cr_7Cd (**1**), Cr_7Mn (**2**), and Cr_7Ni (**3**), by use of spin-Hamiltonian (2), obtained as explained in the text. The numbers in parentheses represent the error on the last significant digit of parameters that were varied to match the experimental spectra.

Cr_7Cd (**1**)	Cr_7Mn (**2**))	Cr_7Ni (**3**)	
g_{Cr}	1.96	1.96	1.96
$g_{M^{II}}$	–	2.00	2.229(5)[a], 2.238(3)[b]
D_{Cr} [cm^{-1}][c]	−0.134(8)	−0.134	−0.134
$D_{M^{II}}$ [cm^{-1}][c]	–	0.04(1)	−1.33(2)
J_{Cr-Cr} [cm^{-1}]	−5.77	−5.77	−5.77
$J_{Cr-M^{II}}$ [cm^{-1}]	–	−6.01	−8.66(6)
D_{Cr-Cr} [cm^{-1}][c]	−0.106(6)	−0.084(9)	−0.106
$D_{Cr-M^{II}}$ [cm^{-1}][c]	–	−0.102(9)	−0.075(9)
Γ_0 [Gauss]	100	100	100

[a] Perpendicular g value. [b] Parallel g value. [c] A Gaussian distribution of standard deviation σ corresponding to 10% of the value of this parameter was used for the reproduction of the very different linewidths observed in the experimental EPR spectra of Cr_7M.

Experimental and simulated single-crystal (K-band) and polycrystalline (X-, K-, Q-bands) spectra of **1** at 5 K are shown in Figures 5 and 6, respectively. In the bottom panel of Figure 5 spectra are shown for an orientation of the external magnetic field nearly normal to the Cr_7Cd plane. In order to obtain the best fit to this spectrum it was necessary to assume a misalignment of 5° of the field with respect to the molecular z axis.[27] In the upper panel of Figure 5 spectra are shown for an orientation of the external magnetic field perpendicular to the molecular z axis, in the plane defined by the eight metal centres. The simulated spectrum was calculated as an equally weighted superposition of eight different contributions, originating from orientations of the

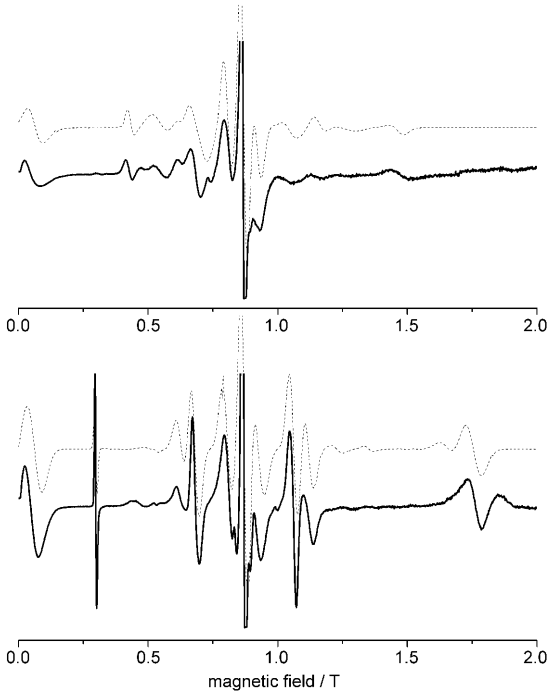

Figure 5. Experimental (——) and simulated (-----) K-band (23.90 GHz) single-crystal EPR spectra of Cr_7Cd (**1**) at 5 K with the external magnetic field in the plane of the ring defined by the metal centres (upper panel) or 5° to the normal to it (lower panel). The simulated spectra were computed by use of spin-Hamiltonian (2) and the relevant parameters in Table 1.

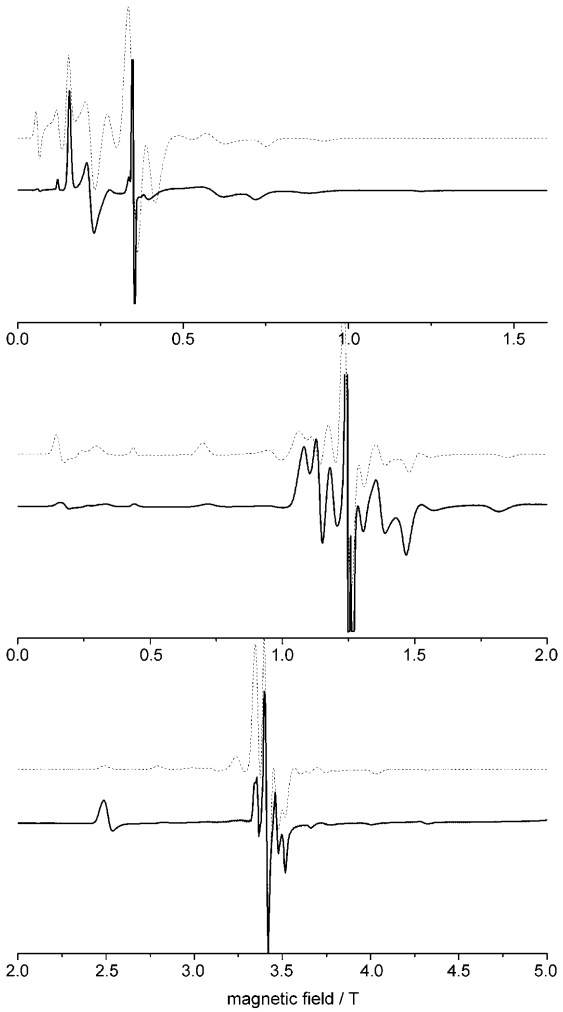

Figure 6. Experimental (——) and simulated (-----) X-band (9.62 GHz, upper panel), Q-band (34.05 GHz, middle panel), and W-band (93.40 GHz, bottom panel) polycrystalline EPR spectra of Cr_7Cd (**1**) recorded at 5, 5, and 10 K, respectively. The simulated spectra were computed by use of spin-Hamiltonian (2) and the relevant parameters in Table 1.

external magnetic field along radii defined by the centre of the "wheel" and each of the eight single-ion sites. This approach was followed to account for the positional disorder of Cr^{III} and M^{II} sites in the crystal lattice and for the uncertainty on the relative orientation of the external magnetic field with respect to the individual single-ion sites in the molecule. This is an assumption since it is evident that there is no special reason for the magnetic field to be oriented along these eight special directions and not along any other eight general in plane directions transforming to each other by 45° rotations about the z molecular axis. The fact that these eight special directions define extrema in the angular variation of the resonance fields for in-plane rotations sets upper limits for the determined D_{Cr} and D_{Cr-Cr} parameters. In addition, the angular variation of the observed resonance fields for in-plane rotations up to $\pm 22.5°$ from these special directions is within 600 G, comparable to the experimental linewidths.

From Figures 5 and 6 one can see that the linewidths of the observed resonances varies considerably over the magnetic field range of the measurement. In order to reproduce these in the simulations it was necessary to use a single natural linewidth $\Gamma_0 = 100$ G, for all observed transitions, with a standard deviation of 10% for D_{Cr} and D_{Cr-Cr} (Figures 5 and 6). Note that the fact that so many experimental band shapes are satisfactorily reproduced at such a wide range of experimental conditions by use of a single natural linewidth and two constant statistical distribution parameters indicates that the linewidth model of Equation (5) is adequate. The disorder introduced in our model by the statistical distribution of the single-ion and exchange anisotropy parameters could originate from the positional disorder of the Cr^{III} and M^{II} sites, by the dynamical hydrogen bonding of the central ammonium ion to the eight fluorides, or by small differences in the single-ion environments across Cr_7M molecules in the crystal lattice.

In Figure 7 is illustrated the assignment of the EPR transitions from a single crystal of **1** at K-band, 5 K, and for an orientation of the magnetic field at an angle of 5° to z. The intense resonances can be described in terms of transitions within the $S = {}^3/_2$ ground spin state and the first two $S = {}^1/_2$ and $S = {}^5/_2$ excited spin states.

The sharp transition marked "a", centred at 2980 G (Figure 7) has a linewidth of about 80 G. This band is attributed to the formally forbidden resonance within the "$\pm {}^3/_2$"

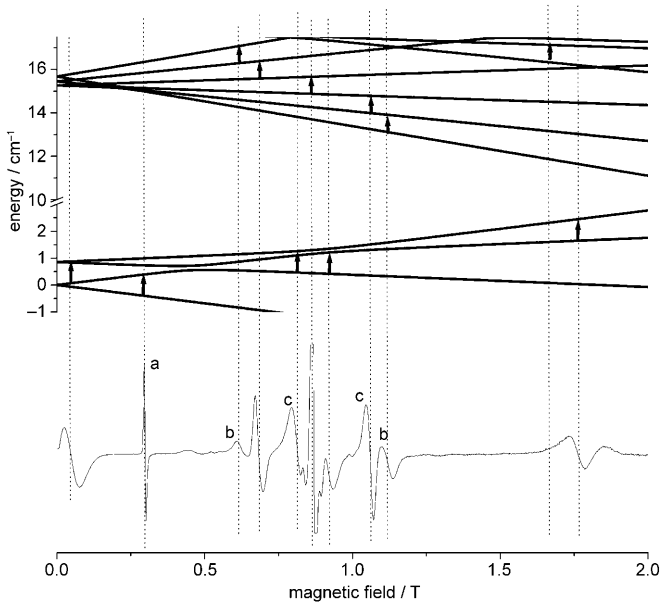

Figure 7. Assignment of the experimentally observed EPR transitions obtained on a single crystal of Cr_7Cd (**1**) at K-band, 5 K, and for an orientation of the external magnetic field of 5° with the molecular z axis. In this Figure the first excited state, of total spin $S=^1/_2$ and of energy 6.67 cm^{-1} above the ground spin state, has been omitted for clarity since it only contributes to intensity in the "$g=2$" spectral region.

Kramers doublet of the ground state. Even when the simulated spectrum is computed for the magnetic field precisely parallel to the molecular z axis, this transition has a non-negligible intensity. The relaxation of the selection rules is due to the asymmetry introduced in **1** by the presence of the diamagnetic Cd^{II} centre that induces a rhombic character to the ground and excited spin states. Since the two eigenstates involved in the transition define a Kramers doublet, and are thus degenerate at zero field, the statistical distribution of D_{Cr} and D_{Cr-Cr} has no contribution to its linewidth via the second term of Equation (5). Consequently, the linewidth depends solely on the first term of Equation (5) and this formally forbidden $\Delta m_s=\pm 3$ transition has a much smaller linewidth than the $\Delta m_s=\pm 1$ transitions in Figure 7.

The four resonances in Figure 7 marked "b" or "c" originate from the $S=^5/_2$ second excited spin state of **1**. The transitions marked "b" have a larger linewidth than those marked "c" (550 and 350 G, respectively). All four transitions correspond to $\Delta m_s=\pm 1$ transitions; consequently, the contribution to the linewidth from the first term of Equation (5) is the same for all four. The differences in linewidth can therefore be attributed to contributions from the second term of Equation (5) via the statistical distribution of the single-ion and exchange anisotropy parameters. Other contributions to line-broadening such as spin relaxation by mixing with other spin states can be disregarded as determining the linewidth differences within this group of four transitions since the effects of S-mixing are of the same order of magnitude for all transitions involving eigenvectors originating from the same spin state.

Interpretation of the EPR spectra of Cr_7Mn: The interpretation of the experimental EPR spectra of **2** was performed in analogy to the methodology presented for **1**. Application of spin-Hamiltonian (2) to the direct product basis set functions of **2** results in a Hermitian matrix of dimension $N=98304$ that we numerically diagonalise as described in the case of **1**. Initially, we used the spin-Hamiltonian parameters determined for **1**, with an isotropic g value for the Mn^{II} centre, $g_{Mn}=2.00$, and an isotropic exchange parameter $J_{Cr-Mn}=J_{Cr-Cr}$. Under these conditions, neglecting the same terms as in the case of **1**, spin-Hamiltonian (2) contains only two free parameters, namely the uniaxial single-ion anisotropy of the Mn^{II} ion, D_{Mn}, and the anisotropic exchange between the Mn^{II} centre and its first neighbour Cr^{III} centres, D_{Cr-Mn}. Following the same approach as for **1**, we attempted to model the experimental EPR spectra of **2** by varying only these two free parameters. The simulations reproduced to a large extent the experimental spectra, but not to the same degree of accuracy as in the case of **1**. Consequently, we allowed D_{Cr-Cr} to vary. This additional degree of freedom allowed us to obtain a satisfactory fit to the experimental spectra of **2**. Finally, the value of the J_{Cr-Mn} was slightly modified to better reproduce the observed intensities of some of the resonances of the experimental spectrum. Small variations of this parameter have a very small effect on the computed resonance fields. The EPR spectra of **2** can satisfactorily be simulated with $D_{Mn}=0.04\ cm^{-1}$, $J_{Cr-Mn}=-6.01\ cm^{-1}$, $D_{Cr-Mn}=-0.102\ cm^{-1}$, and $D_{Cr-Cr}=-0.084\ cm^{-1}$, this later parameter having a value reduced by about 20% with respect to the corresponding value in **1** (Table 1). As in the case of **1**, use of a statistical distribution of the single-ion and exchange anisotropy parameters entering spin-Hamiltonian (2) was necessary to account for the different linewidths of the observed resonances.

Experimental and simulated K- and X-band single-crystal EPR spectra of **2** at 5 K are shown in Figure 8 and 9, respectively. The bottom panels of Figures 8 and 9 show spectra with the external magnetic field nearly normal to the plane defined by the eight metal centres. The upper panels of Figures 8 and 9 show spectra for the magnetic field perpendicular to the molecular z axis, in the plane defined by the eight metal centres. As with **1**, the simulation was calculated as an equally weighted superposition of eight different contributions.

The experimental and simulated K-, Q-, and W-band polycrystalline EPR spectra of **2** obtained at 5, 5, and 10 K respectively, are shown in Figure 10. The high-field region of the experimental W-band spectrum contains resonances characterized by non-regular profiles due to phasing problems. Apart from this small experimental artefact, the experimental spectra are well reproduced by the computed ones.

Figure 11 shows the assignment of the experimentally observed EPR transitions from a single crystal of **2** at K-band, 5 K, with the external magnetic field at an angle of 5° to the molecular z axis. In this Figure only the $S=1$ ground spin state and the $S=2$ first excited spin state are shown for the sake of clarity. The intense resonances of the K-band, 5 K,

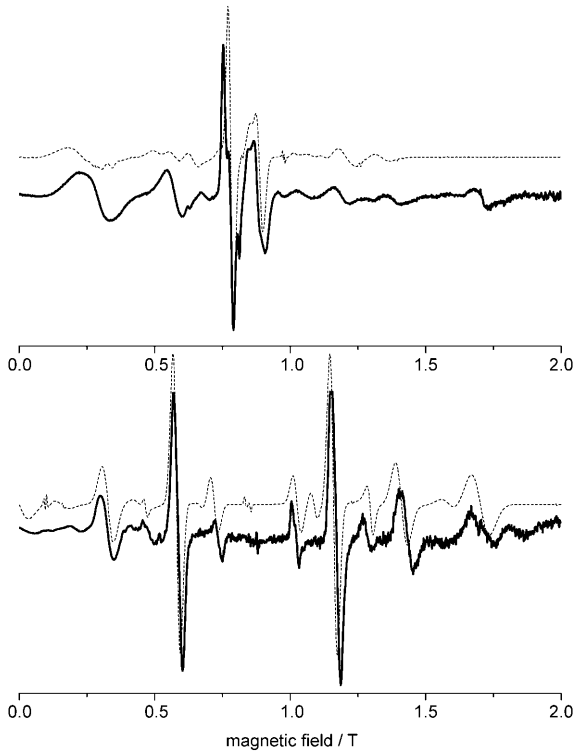

Figure 8. Experimental (——) and simulated (-----) K-band (24.16 GHz) single-crystal EPR spectra of Cr_7Mn (**2**) recorded at 5 K with the external magnetic field in the plane of the ring defined by the metal centres (upper panel) or 5° to the normal to it (lower panel). The simulated spectra were computed by use of spin-Hamiltonian (2) and the relevant parameters in Table 1.

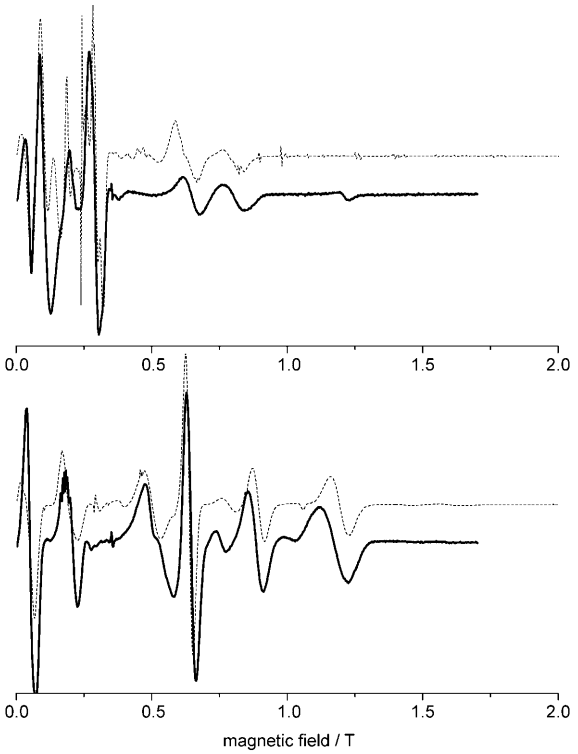

Figure 9. Experimental (——) and simulated (-----) X-band (9.65 GHz) single-crystal EPR spectra of Cr_7Mn (**2**) recorded at 5 K with the external magnetic field in the plane of the ring defined by the metal centres (upper panel) or nearly normal to it (lower panel; misalignment of 5° with respect to the normal). The simulated spectra were computed by use of spin-Hamiltonian (2) and the relevant parameters in Table 1.

EPR spectrum of **2** originate from these two states. Only one transition within the $S=1$ ground spin state is observed, namely the $m_s=0$ to $m_s=+1$ transition. The tail of the $m_s=-1$ to $m_s=0$ transition within the ground spin state can be seen at near zero field as the zero field splitting of the ground spin state is of the same order of magnitude as the excitation quantum.

The four resonances in Figure 11 marked "a" or "b" are $\Delta m_s=\pm 1$ transitions within the $S=2$ first excited spin state of **2**. The transitions marked "a" have a larger linewidth than the transitions "b" (650 and 400 G, respectively). As in the case of **1**, the linewidth difference arises from the second term of Equation (5) which broadens the "a" lines more than the "b" lines.

Interpretation of the EPR spectra of Cr_7Ni: The interpretation of the experimental EPR spectra of **3** was performed in analogy to the methodology presented above for **1** and **2**. At 5 K, the experimental spectra are dominated by the resonance originating from within the $S=^1/_2$ ground spin state (Figure 12). The inset of Figure 12 shows that the ground spin state of **3** is described by an axial g matrix of the effective spin-Hamiltonian (4), as evidenced by the two overlapping bands of the Q-band powder spectrum at around 13850 and 14000 G corresponding to g values of 1.78 and 1.74, respectively. These low g values are a consequence of the tensorial projection of the single-ion g matrices of the Cr^{III} and Ni^{II} sites to the ground spin state of **3**.

The fact that the 5 K experimental EPR spectra of **3** are so dominated by the ground spin-state resonance means that less information is available regarding excited states compared to **1** and **2**. For this reason we have recorded single-crystal K-band EPR spectra of **3** at a temperature of 10 K (Figure 13). Therefore, for **3** the determination of the parameters of spin-Hamiltonian (2) is based on the weak resonances of the single-crystal spectra (Figure 13) because they are much better defined than in polycrystalline spectra (Figure 14). Application of spin-Hamiltonian (2) to the direct product basis set functions of **3** results in a Hermitian matrix of dimension $N=49152$ that we numerically diagonalise as described in the case of **1**. Initially, we use the spin-Hamiltonian parameters determined for **1**, with an isotropic g value for the Ni^{II} centre, $g_{Ni}=2.25$, and an isotropic exchange parameter $J_{Cr-Ni}=J_{Cr-Cr}$. Under these conditions, neglecting the same terms as in the case of **1** and **2**, spin-Hamiltonian (2) contains only two free parameters, namely the uniaxial single-ion anisotropy parameter of the Ni^{II} ion, D_{Ni}, and the uniaxial anisotropic exchange parameter between the Ni^{II} centre and its first neighbour Cr^{III} centres, D_{Cr-Ni}. As in the case of **2**, the obtained simulated spectra reproduced to a large extent the experimental ones but not at a level as satisfactory as in the case of **1** or **2**. Consequently, we al-

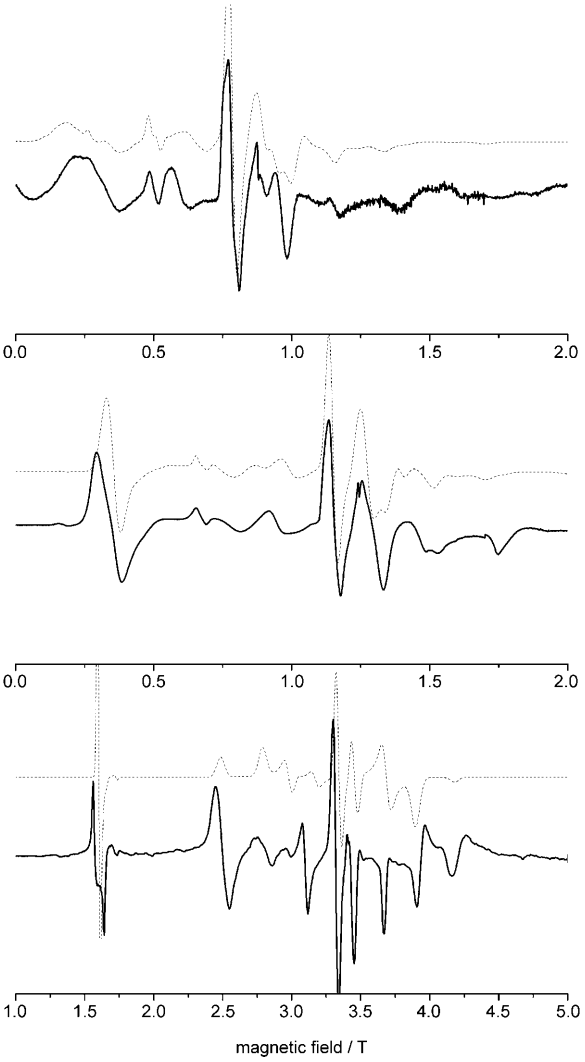

Figure 10. Experimental (——) and simulated (-----) K-band (24.16 GHz, upper panel), Q-band (34.12 GHz, middle panel), and W-band (94.32 GHz, bottom panel) polycrystalline EPR spectra of Cr_7Mn (**2**) recorded at 5, 5, and 10 K, respectively. The simulated spectra were computed by use of spin-Hamiltonian (2) and the relevant parameters in Table 1.

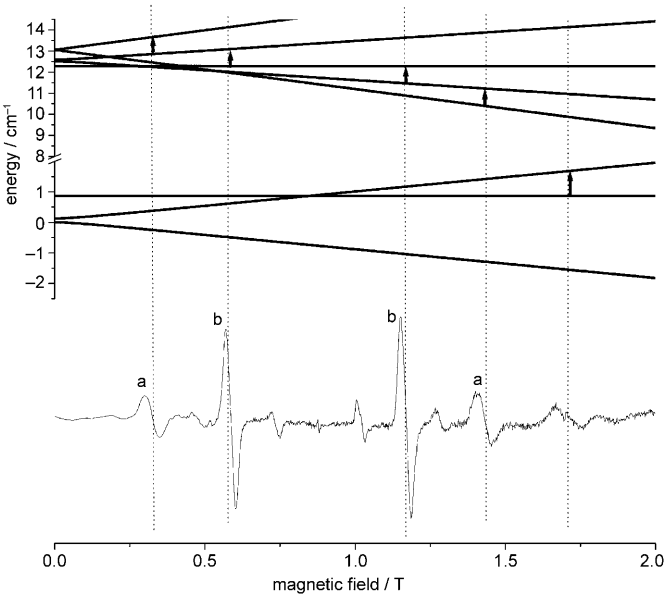

Figure 11. Assignment of the experimentally observed EPR transitions from a single crystal of Cr_7Mn (**2**) at K-band, 5 K, and for an orientation of the external magnetic field making an angle of 5° with the molecular z axis.

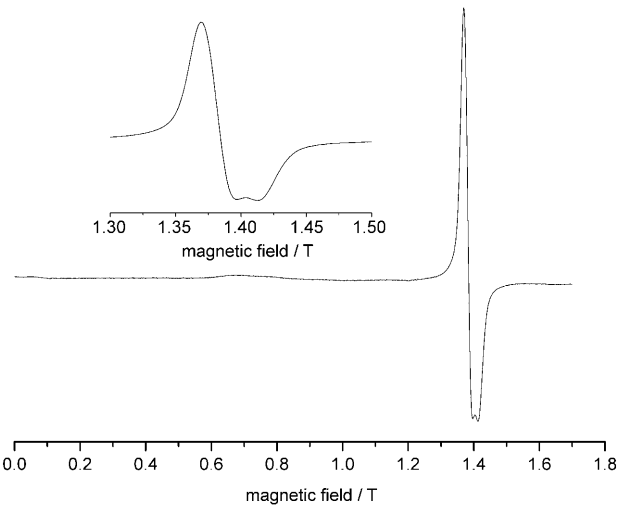

Figure 12. Experimental polycrystalline Q-band (34.08 GHz) EPR spectrum of Cr_7Ni (**3**) at 5 K. The inset shows the axial character of the **g**-matrix of the $S=^1/_2$ ground spin state of **3** as evidenced by the two overlapping bands at around 13850 and 14000 Gauss corresponding to $g=$ 1.78 and 1.74, respectively.

lowed the J_{Cr-Ni} and D_{Cr-Cr} parameters to vary. It was found that variation of the former is necessary to obtain the best agreement, while, variation of the latter parameter is not required. The EPR spectra of **3** can satisfactorily be simulated with $D_{Ni}=-1.33\ cm^{-1}$, $J_{Cr-Ni}=-8.66\ cm^{-1}$, $D_{Cr-Ni}=-0.075\ cm^{-1}$, and $D_{Cr-Cr}=-0.106\ cm^{-1}$. In addition an axial set of g values, $g_{xx,Ni}=g_{yy,Ni}=2.229$, and $g_{zz,Ni}=2.238$, was used for the Ni^{II} site to account for the axial g values of the ground spin state. The best-fit spin-Hamiltonian parameters entering (2) are in Table 1. As in the case of **1** and **2**, use of a statistical distribution of the single-ion and exchange anisotropy parameters in (2) was necessary to account for the different linewidths of the observed resonances.

In the best fit of the single-crystal data for an orientation of the external magnetic field normal to the plane defined by the eight metal centres (Figure 13; lower panel) it was again necessary to assume a small misalignment of 6° with respect to the molecular z axis. As with **1** and **2**, the simulated spectrum for the field in the "Cr_7Ni" plane (Figure 13; upper panel) was calculated as an equally weighted superposition of eight different contributions. Figure 14 shows experimental and simulated Q- and W-band polycrystalline spectra.

Figure 15 illustrates the assignment of the experimentally observed EPR transitions from a single crystal of **3** at K-band and 10 K, with the external magnetic field at an angle

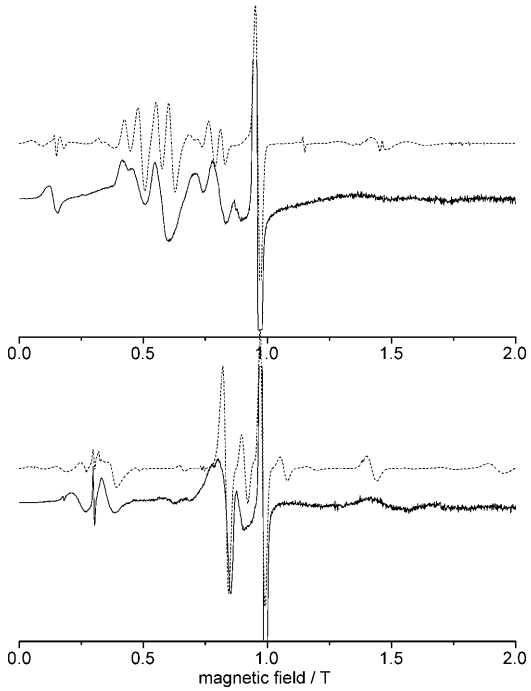

Figure 13. Experimental (——) and simulated (-----) K-band (23.92 GHz) single-crystal EPR spectra of Cr_7Ni (**3**) recorded at 10 K with the external magnetic field in the plane defined by the metal centres (upper panel) or 6° to the normal to it (lower panel). The simulated spectra were computed by use of spin-Hamiltonian (2) and the relevant parameters in Table 1. The ground spin-state resonances have been cropped to better define the excited spin states.

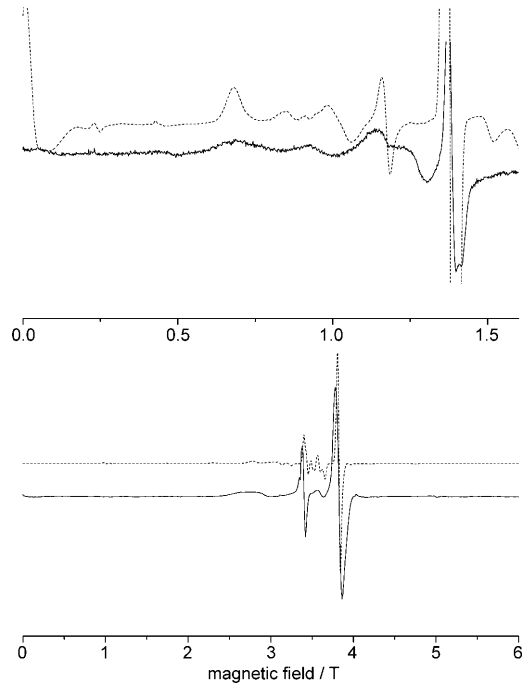

Figure 14. Experimental (——) and simulated (-----) Q-band (34.08 GHz, upper panel) and W-band (93.64 GHz, bottom panel) polycrystalline EPR spectra of Cr_7Ni (**3**) at 10 K. The simulated spectra were computed by use of spin-Hamiltonian (2) and the relevant parameters in Table 1. In the Q-band spectrum the ground spin-state resonances have been cropped to better define the excited spin states.

of 6° with the molecular z axis. The ground spin state, giving rise to the intense resonance at about 1 T, is omitted from this Figure for clarity. Most of the weak resonances originate from the $S=^3/_2$ first excited spin state and the $S=^5/_2$ second excited spin state. Note that diagonalisation of spin-Hamiltonian (2) with the best fit EPR parameters shows that the second excited spin state of **3** is an $S=^5/_2$ spin state. This contrasts with the result obtained using the isotropic spin-Hamiltonian (3) with $J_{Cr-Cr}=J_{Cr-Ni}$, where this $S=^5/_2$ spin state is the third excited spin state (Figure 3). The greater resolution of the EPR spectra, compared with INS, combined with diagonalisation of the more complete Hamiltonian (2) allows us to determine that J_{Cr-Ni} is more anti-ferromagnetic than J_{Cr-Cr} and to show that this stabilizes the $S=^5/_2$ spin state. There is therefore an increase in our understanding of the energy levels in **3**.

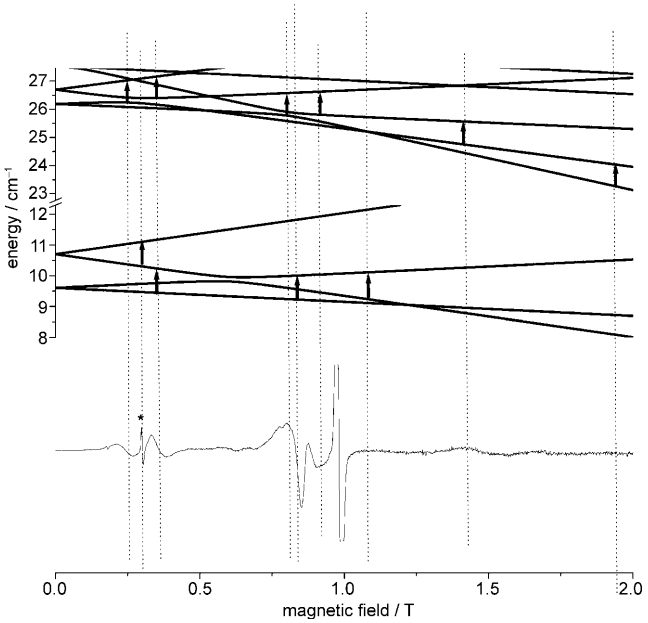

Figure 15. Assignment of the experimentally observed EPR transitions from a single crystal of Cr_7Ni (**3**) at K-band and 10 K, for an orientation of the external magnetic field at an angle of 6° with the molecular z axis. The $S=^1/_2$ ground spin state, giving rise to the resonance centred at ca. 1 T (truncated to better define the excited spin states), has been omitted for clarity of presentation.

From Figure 15 one can conclude, using the same arguments as for **1**, that the $S=^3/_2$ first excited spin state of **3** has a rhombic character, as evidenced by the sharp transition centred at 3000 G marked with "*", originating from within the $m_s=\pm^3/_2$ Kramers doublet.

***S*-mixing effects and spin-Hamiltonian parameters of the individual spin states of Cr_7M**: During the last few years the fact that the spin states of a polynuclear exchange-coupled system admix when the isotropic exchange parameter is not a dominant term of spin-Hamiltonian (2) has received renewed interest in the context of single molecule magnets[20–22] and antiferromagnetically coupled cyclic mole-

cules[9,10e,13,16–18] since such *S*-mixing effects have been shown to play an important role in the static and dynamic magnetic properties of such systems. In order to assess the presence of *S*-mixing effects in Cr_7M, we calculate, by use of the spin-Hamiltonian parameters obtained by the interpretation of the EPR spectra and numerical diagonalisation of the full spin-Hamiltonian (2), the expectation value of the $\hat{\mathbf{S}}^2$ operator for each of the low-lying eigenstates and then solve the equation $\langle\hat{\mathbf{S}}^2\rangle = S(S+1)$ for *S*.

The values of *S* obtained for the forty-two lowest-lying eigenstates of **1**, the forty-two lowest-lying eigenstates of **2**, and the thirty-four lowest-lying eigenstates of **3** are given in Table 2. From Table 2 one can see that the values of *S* for the lowest-lying eigenstates of Cr_7M deviate slightly from half-integer values for **1** and **3** or from integer values for **2**. Analysis of the composition of the eigenvectors obtained by diagonalisation of the anisotropic spin-Hamiltonian (2) showed that the $S=^3/_2$ ground spin state of **1** can be described as being composed of 99.6 and 0.3% from the $S=^3/_2$ ground state and $S=^5/_2$ second excited state, respectively, components of the eigenvectors of the isotropic part of spin-Hamiltonian (2), the remaining contributions coming from mixing with higher excited spin states. For **2**, the $S=1$ ground spin state of the anisotropic spin-Hamiltonian (2) is composed of 99.3 and 0.7% from components of the $S=1$ ground state and $S=2$ first excited spin states, respectively, of the isotropic part of spin-Hamiltonian (2). For **3**, the $S=^1/_2$ ground spin state of the anisotropic spin-Hamiltonian (2) is composed at 99.0, 0.8 and 0.2% from components of the $S=^1/_2$ ground state, $S=^3/_2$ first excited state, and $S=^5/_2$ second excited state, respectively, of the isotropic part of spin-Hamiltonian (2). All the above spin-state compositions are given in terms of squared overlaps and were calculated from $s_{ij}s_{ij}$*, where s_{ij} is the overlap between the *i*th isotropic model and *j*th anisotropic model eigenvectors and * denotes complex conjugation. Hence, the ground states are dominated by a single *S* and can be treated as if *S* is a good, if not exact, quantum number for these eigenstates. However, the increasing deviation from integer or half-integer values of *S* for higher excited spin states (Table 2) shows that *S*-mixing effects are more significant for the higher energy states than for the low-lying ones. This is illustrated in Table 2 where it can be seen that the total spin *S* is a particularly bad label for eigenvectors 11 to 16 of **3**. For the specific spin- Hamiltonian parameters determined in this work, the $m_s=\pm^5/_2$ components of the $S=^5/_2$ second excited spin state of **3** strongly admix with the $S=^1/_2$ third and fourth excited spin states, resulting in significant deviations of the value of *S* from half-integer values for these eigenvectors. Therefore, physics which is dependent on excited states needs to take this *S*-mixing into account.

Given that the spin-Hamiltonian (2) contains single-ion and exchange anisotropy parameters only up to order two, in the absence of *S*-mixing effects the various spin states of Cr_7M would also be characterized by anisotropy parameters only up to order two. However, *S*-mixing effects can induce the presence of terms higher than second order to the effective spin-Hamiltonian (4). Furthermore, in spin-Hamiltonian (2) only uniaxial anisotropy parameters are included. However, the asymmetry introduced in Cr_7M by the presence of the M^{II} centre should induce a rhombic character to the ground and excited spin states. To quantify these effects we followed a numerical fitting approach previously described in the literature.[28] For example in the case of **1**, we numerically diagonalised spin-Hamiltonian (2), with the EPR-derived parameters, to determine the twelve lowest-lying eigenvalues, corresponding to the three lowest spin states ($S=^3/_2, ^1/_2, ^5/_2$), for external magnetic field orientations along the axes of the molecular frame of reference (*xyz*), and for magnetic fields up to 6000 G. For these magnetic fields the eigenvectors describing each of the three lowest spin states do not cross with the ones describing the other two or with higher excited spin states. The field dependence of the ei-

Table 2. Total spin quantum number *S* of each of the forty two low-lying eigenstates of Cr_7Cd (**1**) and Cr_7Mn (**2**), and of the thirty four low-lying eigenstates of Cr_7Ni (**3**), obtained as described in the text.

	S		
Eigenstate	Cr_7Cd (**1**)	Cr_7Mn (**2**)	Cr_7Ni (**3**)
1	1.5048	1.0090	0.5181
2	1.5048	1.0115	0.5181
3	1.5021	1.0030	1.4964
4	1.5021	2.0010	1.4964
5	0.5041	1.9973	1.5026
6	0.5041	1.9955	1.5026
7	2.4987	2.0018	2.4972
8	2.4987	2.0020	2.4972
9	2.4975	0.0185	2.4992
10	2.4975	0.0170	2.4992
11	2.4989	1.0221	1.0243
12	2.4989	1.0413	1.024
13	1.5004	1.1548	2.2099
14	1.5004	2.9927	2.2101
15	0.5100	2.9340	0.682
16	0.5100	2.9845	0.682
17	1.5008	1.0076	1.5002
18	1.5008	2.9982	1.5002
19	0.5212	2.9972	1.5014
20	0.5212	1.0383	1.5014
21	2.4729	2.9964	1.5023
22	2.4728	2.9808	1.5023
23	2.4951	1.0091	1.5015
24	2.4951	2.0009	1.5015
25	2.4412	2.0004	1.5005
26	2.4411	2.0013	1.5005
27	1.6130	2.0004	1.5008
28	1.6129	1.9979	1.5008
29	1.5094	1.9991	1.4987
30	1.5094	2.0016	1.4987
31	1.5220	2.0012	1.5007
32	1.5220	1.9978	1.5007
33	1.2850	1.9991	0.5172
34	1.2847	0.0433	0.5172
35	0.8964	1.0079	
36	0.8969	1.9985	
37	1.5550	1.9913	
38	1.5550	1.9996	
39	1.8149	1.0200	
40	1.8159	1.0066	
41	3.3215	1.9984	
42	3.3221	2.0006	

Table 3. Best-fit spin-Hamiltonian parameters of the effective spin-Hamiltonian (4) for the three lowest-lying eigenstates of Cr_7Cd (**1**), obtained as explained in the text. The numbers in parenthesis represent the error on the last significant digit of the determined parameter.

S	g_{iso}	D [cm^{-1}]	E [cm^{-1}]	B_4^0 [10^{-4} cm^{-1}]	B_4^2 [10^{-4} cm^{-1}]	B_4^4 [10^{-4} cm^{-1}]
$^3/_2$	1.960	−0.41860(3)	−0.04891(3)	–	–	–
$^1/_2$	1.960	–	–	–	–	–
$^5/_2$	1.960	0.06635(3)	0.00344(2)	−1.545(7)	0.85(4)	−0.77(3)

genvalues of each of the three lowest-lying spin states was numerically fitted to the appropriate form of spin-Hamiltonian (4) for orthorhombic symmetry (q = 0, 2, 4), to obtain the spin-Hamiltonian parameters of the individual spin states of **1**. The results are reported in Table 3. From Table 3 one can see that the $S = ^3/_2$ ground state has a non-negligible rhombic character ($E/D = 0.12$). The $S = ^5/_2$ second excited state also has a rhombic character with respect to the second order terms ($E/D = 0.05$) and, in addition, is characterized by non-negligible diagonal and off-diagonal fourth order anisotropy terms. As an illustration of the latter, if only D and E terms are included in spin-Hamiltonian (4) the deviation between experimental and calculated data for the $S = ^5/_2$ state resonances centred at 6290, 6800, 8700, and 11190 G (Figure 7), are about 300, 500, 500 and 200 G, respectively. When fourth order anisotropy terms are included the same deviations are of the order of 10 G. Moreover, inclusion of the fourth-order terms is statistically significant as determined by evaluation of the statistical significance of models containing an increasing number of parameters by means of the F test.[29]

Concerning the origin of these parameters in Hamiltonian (4), we note that the experimental spectra of **1** cannot be fitted by use of spin-Hamiltonian (2) if anisotropic exchange terms are not included because the splittings, at zero field, within the $S = ^5/_2$ second excited spin state (three Kramers doublets successively split by 0.174 and 0.218 cm^{-1}) mainly depend on this parameter. Thus, the inclusion of D_{Cr-Cr} in our spin-Hamiltonian model (2) is justified by the experimental data. In addition, because spin-Hamiltonian (4) is not able to reproduce the transitions within this state if fourth order anisotropy terms are not included, these terms can also be mainly attributed to contributions from the anisotropic exchange of spin-Hamiltonian (2). Such exchange controlled higher order terms in the GSA spin-Hamiltonian are in agreement with what has been previously shown by Barra et al.,[11] by Hendrickson and Hill et al.,[21] and with the fact that the single-ion second order anisotropy terms of (2) can not project, at least to first order, to fourth order spin-state anisotropy terms.

The spin-Hamiltonian parameters of the effective spin-Hamiltonian (4) of the individual spin states of **2** and **3** were obtained following a similar approach as in the case of **1**. The results for the $S = 1$ ground spin state and the $S = 2$ first excited spin state of **2** are reported in Table 4. The $S = 1$ ground spin state of **2** has a non-negligible rhombic character ($E/D = 0.08$). This is also true for the $S = 2$ first excited spin state which is also characterized by a diagonal fourth order anisotropy term. Unlike in the case of **1**, for **2** the presence of fourth order off-diagonal terms in spin-Hamiltonian (4) describing the first excited spin state is not strongly statistically significant. The parameters of the effective spin-Hamiltonian (4) of the $S = ^1/_2$ ground and the $S = ^3/_2$ first excited spin states of **3** are reported in Table 5. Axial g values are used, in accordance with the experimental data. The $S = ^3/_2$ first excited spin state of **3** has a rhombic anisotropy ($E/D = 0.08$). The $S = ^5/_2$ second excited spin state overlaps in energy with the $S = ^1/_2$ third excited spin state, hence determination of the effective spin-Hamiltonian parameters of these two spin states is not possible following the methodology described for **1** and **2**.

Table 4. Best-fit spin-Hamiltonian parameters of the effective spin-Hamiltonian (4) for the two lowest-lying eigenstates of Cr_7Mn (**2**), obtained as explained in the text. The numbers in parenthesis represent the error on the last significant digit of the determined parameter.

S	g_{iso}	D [cm^{-1}]	E [cm^{-1}]	B_4^0 [10^{-4} cm^{-1}]
1	1.960	−0.806(2)	−0.065(1)	–
2	1.960	0.1836(3)	−0.0122(2)	−7.2(1)

Table 5. Best-fit spin-Hamiltonian parameters of the effective spin-Hamiltonian (4) for the two lowest-lying eigenstates of Cr_7Ni (**3**), obtained as explained in the text. The numbers in parenthesis represent the error on the last significant digit of the determined parameter.

S	g_{xx}, g_{yy}	g_{zz}	D [cm^{-1}]	E [cm^{-1}]
$^1/_2$	1.784(3)	1.744(3)	–	–
$^3/_2$	1.916(2)	1.920(1)	0.5445(1)	0.0418(1)

We now comment on the assumptions made concerning the parameters used in spin-Hamiltonian (2). Given that a model including axial single-ion and exchange anisotropy terms is sufficient to induce the presence of both second order rhombic anisotropy terms and fourth order anisotropy terms in spin-Hamiltonian (4), we are able to neglect single-ion rhombic anisotropy terms in the model. Taking these latter terms into account would simply result in an extra parameter having an indiscernible effect with the parameters already included. Also, we note that the interpretation of INS spectra[9] obtained on Cr_7M did not require introduction of the anisotropic exchange interaction terms in the spin-Hamiltonian model used because of the lower resolution of INS compared to EPR. Consequently, the single-ion anisotropy terms of Cr_7M determined by INS studies[9] should be understood as expressing the combined effect of both single-ion and anisotropic exchange contributions.

Finally, we compare the approach presented in this work to the determination of the spin-Hamiltonian parameters of

spin-Hamiltonian (2) by an approach based on the use of projection coefficients[3] within the strong exchange limit. The relevant projection coefficients of the various spin-states of Cr_7M were determined numerically from the eigenvectors obtained by numerical diagonalisation of the isotropic spin-Hamiltonian (3) considering only first neighbour exchange interactions of $-5.77\ cm^{-1}$ between all paramagnetic centres. For the $S=^3/_2$ ground and $S=^5/_2$ second excited spin state of **1** we obtain: $D_{3/2}=1.3572\,D_{Cr}+2.0574\,D_{Cr-Cr}$ and $D_{5/2}=-0.1224\,D_{Cr}-0.5100\,D_{Cr-Cr}$ from which, using the appropriate values from Table 3, $D_{Cr}=-0.175\ cm^{-1}$ and $D_{Cr-Cr}=-0.088\ cm^{-1}$ are obtained. These values are in good agreement with those from Hamiltonian (2) (Table 1). For the $S=1$ ground and $S=2$ first excited spin-state of **2** we obtain: $D_1=2.0235\,D_{Cr}+1.4574\,D_{Mn}+3.4966\,D_{Cr-Cr}+2.2850\,D_{Cr-Mn}$ and $D_2=-0.5678\,D_{Cr}+00548\,D_{Mn}-1.0959\,D_{Cr-Cr}-0.2718\,D_{Cr-Mn}$ from which, using the appropriate values from Table 4, $D_{Mn}=-0.129\ cm^{-1}$ and $D_{Cr-Mn}=0.019\ cm^{-1}$ are obtained after setting $D_{Cr}=-0.175\ cm^{-1}$ and $D_{Cr-Cr}=-0.088\ cm^{-1}$. This value of single-ion anisotropy for Mn^{II} is of similar magnitude to that for Cr^{III} and the anisotropic exchange parameter between Cr^{III} and Mn^{II} is of lower magnitude and opposite sign than that between Cr^{III} sites, in contrast to the results from Hamiltonian (2) in Table 1. However, the above parameters involving the Mn^{II} site are extremely sensitive to the parameters determined from **1**. For example, changing D_{Cr-Cr} from -0.088 to $-0.078\ cm^{-1}$ leads to $D_{Mn}=-0.098\ cm^{-1}$ and $D_{Cr-Mn}=-0.016\ cm^{-1}$, showing that a small variation of the parameters of **1** is sufficient to even change the sign of the determined anisotropic exchange parameters. If we take into account that in the presence of anisotropic Hamiltonian terms the projection coefficients will vary resulting in different parameters again, and also the arguments relating to the origin of the fourth order terms and the number of free parameters included in the model, we conclude that direct use of the eigenvectors of the anisotropic spin-Hamiltonian (2) greatly simplifies the analysis of the spectroscopic data for Cr_7M.

Conclusion

We presented here a theoretical methodology for the interpretation of EPR spectra of polymetallic exchange-coupled systems characterized by spin-Hamiltonian matrices of such large dimension that they are not possible to manipulate by numerical full-matrix diagonalisation algorithms because of unrealistic computational time and memory storage requirements. We have shown that the interpretation of the low temperature spectroscopic properties of such systems can be achieved by use of restricted size effective subspaces derived by a rigorous solution of the eigenvalue problem for the full spin-Hamiltonian of the studied systems. Analysis of the highly resolved EPR spectra of Cr_7M allowed for the direct quantification of the contributions of single-ion and exchange anisotropy terms to the magnetic properties of the studied systems, the latter term being the sum of through space dipolar and through bond anisotropic interactions.

As can be seen from the parameters reported in Table 1, we have shown that in the family of the Cr_7M complexes the transferability of spin-Hamiltonian parameters across complexes of the family is possible. Only in the case of the anisotropic exchange contributions between Cr^{III} centres in **2** it was necessary to use a value about 20% lower to that dictated by the transferability of parameters. However, such a variation is not extreme. The fact that the parameters of spin-Hamiltonian (2) are transferable between complexes of the series demonstrates the validity of the used spin-Hamiltonian model for the description of these polymetallic exchange coupled systems. The small number of parameters used in this work determines the behaviour of ground and excited spin states of various integer and half-integer total spin S and is sufficient for the interpretation of low temperature EPR data of single crystals and polycrystalline samples at excitation frequencies from X- to W-band and all that in the presence of S-mixing effects.

The anisotropic exchange parameters determined in this work are of the order of $-0.1\ cm^{-1}$. This is almost the double the estimated magnetic dipole spin–spin exchange contributions to the anisotropic exchange terms, meaning that the through bond anisotropic exchange contributions are of the same order of magnitude as the magnetic dipole spin–spin exchange terms. Similar surprisingly large contributions from through-bond anisotropic exchange terms have been reported in a very detailed single-crystal EPR study of an Fe^{III} binuclear complex where it was shown that the through bond anisotropic exchange contributions are of the same order of magnitude as the dipolar ones even for a relatively isotropic centre as the Fe^{III} ion.[2b] However it has to be mentioned here that the above arguments are only valid under the assumption that the point dipole approximation perfectly covers the physics of the spin–spin coupling term.

In this work we obtain slightly different spin-Hamiltonian parameters for **1**, **2**, and **3** compared to the ones obtained by previous INS studies.[9] We tested the parameters of spin-Hamiltonian (2) obtained in this work by using them for the calculation, by home-written software, of the INS spectra of "Cr_7M" in the same conditions as the reported experimental spectra. The computed INS spectra of **1**, **2**, and **3**, as well as their Q-dependences, shown in the Supporting Information section, are in excellent agreement with the experimental spectra given in reference [9].

We have shown, in agreement with previous studies,[9] that S-mixing effects have to be taken into account for a full description of the magnetic properties of the Cr_7M complexes in general. The ground spin states of Cr_7M are only admixed to 0.3 to 1% with excited spin states. However, the effects of the minor S-mixing on the EPR spectra are not negligible, particularly in the low-lying excited spin states where the calculated resonance fields shift by about 500 G in the example of the second excited state of **1** and by about 200 to 800 G for the first excited state of **2**, when S-mixing is taken into account. An equivalent conclusion about reso-

nance magnetic fields has been reached in a previous study of an hexanuclear cyclic Fe^{III} complex by Pilawa et al.[5] *S*-mixing effects of the order of 2.6%, thus of the same order of magnitude as the ones determined in this study, have even been shown to lift the spin-forbidden character of intermultiplet EPR transitions in a nonanuclear Mn^{II} complex. These were observed in single crystals at 1.4 K between the $m_s = -5/2$ and $m_s = -7/2$ levels of the $S = 5/2$ ground and $7/2$ first excited states, respectively, at about 6 T and 60 GHz.[6] In the work presented here only intramultiplet EPR transitions have been observed in the explored field-frequency ranges, up to 6 T and 95 GHz. In order to test whether such transitions could occur we have calculated EPR spectra of **1** to higher field-frequencies (e.g. Figure S1, Supporting Information): the intermultiplet transition between the $m_s = -3/2$ and $m_s = -5/2$ components of the $S = 3/2$ ground state and $S = 5/2$ second excited state is predicted to become weakly allowed, at about 10.55 T for 180 GHz with the magnetic field parallel to the molecular *z* axis. Direct evidence for an anticrossing between these states, at about 16 T, has been observed by torque magnetometry and INS.[16,17] The calculated intensity of this intermultiplet transition is only about 1% of that of the allowed $m_s = -3/2$ to $m_s = -1/2$ transition within the $S = 3/2$ ground state. This is weaker than the intermultiplet EPR transition in Mn_9[6] presumably due to the smaller extent of *S*-mixing (by roughly one order of magnitude) and the intrinsic higher transition probability of an $m_s = -5/2$ to $m_s = -7/2$ transition. For complex **3**, the mixing between ground and excited spin states of about 1%, determined in this study, is in good agreement with that previously determined from modelling INS data.[9] A detailed study of the influence of *S*-mixing effects on the low-temperature spin-dynamics of **3**, and its suitability as a prototype cluster qubit, has been presented elsewhere.[18a]

Finally, in this work we show that the spin-Hamiltonian parameters of Cr_7M do not have sharply defined values but are rather distributed around a mean value following a statistical distribution, assumed to be Gaussian, of standard deviation of about 10% of the value of the mean. The source of this disorder may be due to the positional disorder of the Cr^{III} and M^{II} sites in Cr_7M, or small differences of the single-ion environment across molecules, as discussed in previous sections. Cluster environment inhomogeneity effects have been proposed to contribute to the echo-detected EPR spectrum of 3,[19] where in addition it was shown that the longitudinal relaxation time of the ground spin state of **2** presents a dependence on the magnetic anisotropy of the ground spin state, probably through spectral diffusion effects.[19] Thus, the statistically distributed nature of the spin-Hamiltonian parameters of Cr_7M should be taken into account in dynamic magnetization studies of these compounds since it leads to a statistically distributed ground spin-state anisotropy.

Experimental Section

The Cr_7M molecules were prepared as reported elsewhere.[7] These recrystallize as dark green plates with tetragonal (*P*4) symmetry, with the molecules lying on a four-fold axis: see ref.[1] for unit cell details. EPR spectra at X- (ca. 9.5), K- (ca. 24), and Q-band (ca. 34 GHz) frequencies were measured on a Bruker ESP 300E spectrometer. Magnetic fields and microwave frequencies were independently calibrated. Single crystals were mounted on quartz studs with machined faces to allow measurement at selected orientations with respect to the applied magnetic field. W-band (ca. 94 GHz) EPR spectra were recorded on a home-built instrument.[30]

Acknowledgement

This work was supported by the EPSRC (UK), the Deutsche Forschungsgemeinschaft priority program 1137 "Molecular Magnetism", the Marie Curie Intra-European Fellowships (MEIF-CT-2005-024897), the European Commission Network of Excellence "MAGMANet" and the Danish Natural Science Research Council (Steno grant 272-07-0147).

[1] a) S. Kremer, *Inorg. Chem.* **1985**, *24*, 887; b) J. Glerup, S. Larsen, H. Weihe, *Acta Chem. Scand.* **1993**, *47*, 1154; c) J. Glerup, H. Weihe, *Inorg. Chem.* **1997**, *36*, 2816.
[2] a) A. Ozarowski, B. R. McGarvey, J. E. Drake, *Inorg. Chem.* **1995**, *34*, 5558; b) P. ter Heerdt, M. Stefan, E. Goovaerts, A. Caneschi, A. Cornia, *J. Magn. Reson.* **2006**, *179*, 29.
[3] A. Bencini, D. Gatteschi, *EPR of Exchange Coupled Systems*, Springer, Berlin, **1989**.
[4] G. L. Abbati, L.-C. Brunel, H. Casalta, A. Cornia, A. C. Fabretti, D. Matteschi, A. K. Hassan, A. G. M. Jansen, A. L. Maniero, L. Pardi, C. Paulsen, U. Segre, *Chem. Eur. J.* **2001**, *7*, 1796.
[5] B. Pilawa, I. Keilhauer, G. Fischer, S. Knorr, J. Rahmer, A. Grupp, *Eur. Phys. J. B* **2003**, *33*, 321.
[6] S. Datta, O. Waldmann, A. D. Kent, V. A. Milway, L. K. Thompson, S. Hill, *Phys. Rev. B* **2007**, *76*, 052407.
[7] F. K. Larsen, E. J. L. McInnes, H. El Mkami, J. Overgaard, S. Piligkos, G. Rajaraman, E. Rentschler, A. A. Smith, G. M. Smith, V. Boote, M. Jennings, G. A. Timco, R. E. P. Winpenny, *Angew. Chem.* **2003**, *115*, 105; *Angew. Chem. Int. Ed.* **2003**, *42*, 101.
[8] S. Carretta, J. van Slageren, T. Guidi, E. Liviotti, C. Mondelli, D. Rovai, A. Cornia, A. L. Dearden, F. Carsughi, M. Affronte, C. D. Frost, R. E. P. Winpenny, D. Gatteschi, G. Amoretti, R. Caciuffo, *Phys. Rev. B* **2003**, *67*, 094405.
[9] R. Caciuffo, T. Guidi, G. Amoretti, S. Carretta, E. Liviotti, P. Santini, C. Mondelli, G. Timco, C. A. Muryn, R. E. P. Winpenny, *Phys. Rev. B* **2005**, *71*, 174407.
[10] a) B. Normand, X. Wang, X. Zotos, D. Loss, *Phys. Rev. B* **2001**, *63*, 184409; b) C. Raghu, I. Rudra, D. Sen, S. Ramasesha, *Phys. Rev. B* **2001**, *64*, 064419; c) I. Rudra, S. Ramasesha, D. Sen, *Phys. Rev. B* **2002**, *66*, 014441; d) N. Regnault, T. Jolicoeur, R. Sessoli, D. Gatteschi, M. Verdaguer, *Phys. Rev. B* **2002**, *66*, 054490; e) E. Liviotti, S. Carretta, G. Amoretti, *J. Chem. Phys.* **2002**, *117*, 3361; f) S. Carretta, P. Santini, E. Liviotti, N. Magnani, T. Guidi, R. Caciuffo, G. Amoretti, *Eur. Phys. J. B* **2003**, *36*, 169; g) T. Guidi, S. Carretta, P. Santini, E. Liviotti, N. Magnani, C. Mondelli, O. Waldmann, L. K. Thompson, L. Zhao, C. D. Frost, G. Amoretti, R. Caciuffo, *Phys. Rev. B* **2004**, *69*, 104432; h) G. Chaboussant, A. Sieber, S. Ochsenbein, H.-U. Güdel, M. Murrie, A. Honecker, N. Fukushima, B. Normand, *Phys. Rev. B* **2004**, *70*, 104422; i) O. Waldmann, H. U. Güdel, *Phys. Rev. B* **2005**, *72*, 094422.
[11] A.-L. Barra, A. Caneschi, A. Cornia, D. Matteschi, L. Gorini, L.-P. Heiniger, R. Sessoli, L. Sorace, *J. Am. Chem. Soc.* **2007**, *129*, 10754.

[12] a) E. R. Davidson, *J. Comp. Phys.* **1975**, *17*, 87; b) B. Liu, *Technical Report LBL-8158*; Lawrence Berkeley Laboratory, University of California, Berkeley CA, **1978**.

[13] S. Piligkos, E. Bill, D. Collison, E. J. L. McInnes, G. A. Timco, H. Weihe, R. E. P. Winpenny, F. Neese, *J. Am. Chem. Soc.* **2007**, *129*, 760.

[14] N. V. Gerbeleu, Yu. T. Struchkov, G. A. Timco, A. S. Batsanov, K. M. Indrichan, G. A. Popovich, *Dokl. Akad. Nauk SSSR* **1990**, *313*, 1459.

[15] J. van Slageren, R. Sessoli, D. Gatteschi, A. A. Smith, M. Helliwell, R. E. P. Winpenny, A. Cornia, A-L. Barra, A. G. M. Jansen, E. Rentschler, G. A. Timco, *Chem. Eur. J.* **2002**, *8*, 277.

[16] S. Carretta, P. Santini, G. Amoretti, M. Affronte, A. Ghirri, I. Sheikin, S. Piligkos, G. Timco, R. E. P. Winpenny, *Phys. Rev. B* **2005**, *72*, 060403.

[17] S. Carretta, P. Santini, G. Amoretti, T. Guidi, J. R. D. Copley, Y. Qiu, R. Caciuffo, G. Timco, R. E. P. Winpenny, *Phys. Rev. Lett.* **2007**, *98*, 167401.

[18] a) F. Troiani, A. Ghirri, M. Affronte, S. Carretta, P. Santini, G. Amoretti, S. Piligkos, G. Timco, R. E. P. Winpenny, *Phys. Rev. Lett.* **2005**, *94*, 207208; b) M. Affronte, F. Troiani, A. Ghirri, A. Candini, M. Evangelisti, V. Corradini, S. Carretta, P. Santini, G. Amoretti, F. Tuna, G. Timco, R. E. P. Winpenny, *J. Phys. D Appl. Phys.* **2007**, *40*, 2999.

[19] A. Ardavan, O. Rival, J. J. L. Morton, S. J. Blundell, A. M. Tyryshkin, G. A. Timco, R. E. P. Winpenny, *Phys. Rev. Lett.* **2007**, *98*, 057201.

[20] S. Carretta, E. Liviotti, N. Mangani, P. Santini, G. Amoretti, *Phys. Rev. Lett.* **2004**, *92*, 207205.

[21] A. Wilson, J. Lawrence, E-C. Yang, M. Nakano, D. N. Hendrickson, S. Hill, *Phys. Rev. B* **2006**, *74*, 140403.

[22] a) C. J. Milios, A. Vinslava, W. Wernsdorfer, S. Moggach, S. Parsons, S. P. Perlepes, G. Christou, E. K. Brechin, *J. Am. Chem. Soc.*, **2007**, *129*, 2754; b) C. J. Milios, A. Vinslava, W. Wernsdorfer, A. Prescimone, P. A. Wood, S. Parsons, S. P. Perlepes, G. Christou, E. K. Brechin, *J. Am. Chem. Soc.*, **2007**, *129*, 6547; c) C. J. Milios, R. Inglis, A. Vinslava, R. Bagai, W. Wernsdorfer, S. Parsons, S. P. Perlepes, G. Christou, E. K. Brechin, *J. Am. Chem. Soc.*, **2007**, *129*, 12505; d) S. Piligkos, J. Bendix, H. Weihe, C. J. Milios, E. K. Brechin, *Dalton Trans.* **2008**, 2277; e) S. Carretta, T. Guidi, P. Santini, G. Amoretti, O. Pieper, B. Lake, J. van Slageren, F. El Hallak, W. Wernsdorfer, H. Mutka, M. Russina, C. J. Milios, E. K. Brechin, *Phys. Rev. Lett.* **2008**, *100*, 157203.

[23] a) U. Fano, G. Racah, *Irreducible Tensorial Sets*, Academic Press, New York, **1959**; b) J. S. Griffith, *The Irreducible Tensor Method for Molecular Symmetry Groups*, Prentice Hall, Englewood Cliffs, NJ, **1962**; c) B. L. Silver, *Irreducible Tensor Methods*, Academic Press, New York, **1976**.

[24] A. Abragam, B. Bleaney, *Electron Paramagnetic Resonance of Transition Ions*, Dover, New York, **1986**.

[25] S. K. Klitgaard, F. Galsbøl, H. Weihe, *Spectrochim. Acta Part A* **2006**, *63*, 836.

[26] a) J. Glerup, H. Weihe, *Acta Chem. Scand.* **1991**, *45*, 444; b) C. J. Jacobsen, E. Pedersen, J. Villadsen, H. Weihe, *Inorg. Chem.* **1993**, *32*, 1216; c) P. L. W. Tregenna-Piggott, H. Weihe, J. Bendix, A. L. Barra, H. U. Güdel, *Inorg. Chem.* **1999**, *38*, 5928; d) S. Mossin, M. Stefan, P. ter Heerdt, A. Bouwen, E. Goovaerts, H. Weihe, *Appl. Magn. Reson.* **2001**, *21*, 587.

[27] This misalignment is seen for all compounds and is possibly due to deviation of the orientation of the sample tube (and hence the rotation axis), containing the crystal mounted on a vertical surface of a quartz stud, from true vertical, the accuracy of which is limited by the spectrometer design as well as from the manual mounting.

[28] A. Bencini, I. Ciofini, G. M. Uytterhoeven, *Inorg. Chim. Acta* **1998**, *274*, 90.

[29] W. H. Press, B. P. Flannery, S. A. Teukolsky, W. T. Vetterling, *Numerical Recipes in C. The Art of Scientific Computing*, Cambridge University Press, Cambridge, **1988**.

[30] G. M. Smith, J. C. G. Lesurf, R. H. Mitchell, P. C. Riedi, *Rev. Sci. Instrum.* **1998**, *69*, 3924.

Received: September 15, 2008
Published online: February 6, 2009

